Quantum control of rovibrational dynamics and application to light-induced molecular chirality

Monika Leibscher,[1] Eugenio Pozzoli,[2] Alexander Blech,[1] Mario Sigalotti,[3] Ugo Boscain,[3] and Christiane P. Koch[1,*]

[1]*Dahlem Center for Complex Quantum Systems and Fachbereich Physik, Freie Universität Berlin, Arnimallee 14, 14195 Berlin, Germany*

[2]*IRMAR, UMR No. 6625, CNRS, Université de Rennes, 35000 Rennes, France*

[3]*Laboratoire Jacques-Louis Lions, Sorbonne Université, Université de Paris, CNRS, Inria, 75005 Paris, France*

(Received 19 October 2023; accepted 18 December 2023; published 16 January 2024)

Achiral molecules can be made temporarily chiral by excitation with electric fields, in the sense that an average over molecular orientations displays a net chiral signal [D. S. Tikhonov *et al.*, Sci. Adv. **8**, eade0311 (2022)]. Here, we go beyond the assumption of molecular orientations to remain fixed during the excitation process. Treating both rotations and vibrations quantum mechanically, we identify conditions for the creation of chiral vibrational wave packets, with net chiral signals, in ensembles of achiral molecules which are initially randomly oriented. Based on the analysis of symmetry and controllability, we derive excitation schemes for the creation of chiral wave packets using a combination of (a) microwave and IR pulses and (b) a static field and a sequence of IR pulses. These protocols leverage quantum rotational dynamics for pump-probe spectroscopy of chiral vibrational dynamics, extending the latter to regions of the electromagnetic spectrum other than the UV.

DOI: 10.1103/PhysRevA.109.012810

I. INTRODUCTION

The insight that molecular chirality may be explored in gas phase ensembles of molecules with random orientations [1,2] has triggered a surge of experimental activity, and chiral molecules interacting with light in the electric dipole approximation have become a central focus of current atomic, molecular, and optical research, both experimental [3–9] and theoretical [10–18]. Methods like photoelectron dichroism [1,3,9,19–22], chiral-sensitive high-harmonic generation [23], laser-induced enantiomer selective molecular orientation [6,12], and microwave three-wave mixing [2,4,5,7,8,24] allow one to discriminate between enantiomers of chiral molecules in the gas phase. At the same time, it is not yet clear what ultimately determines the magnitude of these chiral signatures. One way to approach this question is to imprint chirality onto achiral molecules [25,26] or atoms [27–31].

For example, an achiral molecule can become temporarily chiral if the nuclei are distorted from their achiral equilibrium configuration by exciting nuclear vibrations and the oscillation between chiral and achiral structures can be measured by photoelectron circular dichroism [26]. When starting from a planar molecule, Raman excitation of an out-of-plane normal mode in the presence of a static electric field has been proposed to create a chiral vibrational wave packet [26]. In general, the interaction of three orthogonal components of the molecular (transition) dipole moment with electric fields with three orthogonal polarization directions is sufficient to induce chirality in an achiral structure and yield a net chiral signal when averaged over random orientations [26]. This is in full analogy to the conditions for enantiomer-selective response in a sample of randomly oriented chiral molecules with light-matter interaction in the electric dipole approximation [32]. In both cases [26,32], the conditions for enantiomer sensitivity have been derived under the assumption that molecular rotations are frozen during the interaction and can be described by a classical probability distribution over Euler angles. For ultrafast Raman excitation, this is a valid assumption but rotations and vibrations can also be driven by much slower processes, e.g., by long, narrowband IR pulses. In the latter case, the molecules rotate while external fields excite molecular vibrations, and the rotation affects even purely vibrational observables. On the one hand, the rotation may result in decoherence of the vibrational superpositions. On the other hand, it may allow for new excitation processes to create chiral vibrational wave packets. Here we identify and describe these new routes to imprint temporal chirality onto achiral molecules. To this end, we present a full quantum-mechanical treatment of the rovibrational dynamics which allows us to generalize the conditions for creating temporal chiral structures to rotating molecules and to distinguish between classical and quantum-mechanical routes to induce chirality.

In order to determine the conditions for creating chirality in randomly rotating molecules, we apply two methods. (i) We employ the symmetry properties of asymmetric top rotors [33], extending an earlier symmetry analysis for rigid chiral molecules [14] to rovibrational dynamics. (ii) We analyze the controllability of a vibrating quantum rotor. Controllability analysis answers the question whether it is possible to reach a control target with a given set of external fields [34]. Analyzing the controllability of rotational systems is challenging due to the inherent degeneracies. In the rigid rotor limit where vibrations are ignored, controllability properties have been derived for linear rotors [35–37] as well as symmetric [38,39] and asymmetric tops [40–42]. Recently developed graphical methods to analyze the controllability [43–45] have been

*Corresponding author: christiane.koch@fu-berlin.de

proven helpful to analyze controllability of quantum rotors [40,41]. Here we apply these methods to vibrating rotors. This analysis allows us to identify the new excitation processes for the creation of chiral vibrational wave packets which we verify by numerical simulations of the rovibrational dynamics.

The paper is organized as follows. In Sec. II we present the theoretical framework for describing vibrational observables in a driven rovibrational quantum system. General conditions for exciting coherent vibrational wave packets in randomly oriented molecules based on the symmetry as well as the formulation of the control problem are discussed in Sec. III. In Secs. IV and V we present two different strategies to create a chiral vibrational wave packet. The first scheme combines a purely rotational excitation using microwave pulses with an IR pulse that induces rovibrational transitions. This scheme is described in Sec. IV. In Sec. V we demonstrate that a chiral wave packet can also be excited with three IR pulses in combination with a static electric field. In Sec. VI we summarize our findings.

II. VIBRATIONAL WAVE PACKETS IN ROTATING MOLECULES: THEORETICAL FRAMEWORK

In order to describe vibrational excitation in randomly oriented molecules, we model the molecular Hamiltonian as

$$H_0 = \sum_{\nu}\sum_{j}\left(E_{\nu}^{\mathrm{vib}} + E_{j}^{\mathrm{rot}}\right)|\nu\rangle|\phi_j\rangle\langle\phi_j|\langle\nu|, \tag{1}$$

where we neglect any rovibrational coupling. We consider a single vibrational mode, represented by the operator $\hat{\chi}$, and the vibrational eigenstates $|\nu\rangle$ along this normal. The eigenstates of a rigid top are denoted by $|\phi_j\rangle$, where j indicates the quantum numbers of the rigid rotor. The vibrational energies are denoted by E_{ν}^{vib}, and E_{j}^{rot} are the eigenvalues of the rigid rotor. The molecules evolve according to the time-dependent Schrödinger equation

$$i\hbar\frac{\partial}{\partial t}|\psi(t)\rangle = [H_0 + H_{\mathrm{int}}(t)]|\psi(t)\rangle. \tag{2}$$

The interaction between the molecules and a set of electric fields

$$\mathbf{E}_i = \boldsymbol{e}_i\mathcal{E}_i u_i(t) \tag{3}$$

is described in the electric dipole approximation as

$$H_{\mathrm{int}}(t) = -\sum_i u_i(t)H_i, \tag{4}$$

with

$$H_i = \mathcal{E}_i\boldsymbol{\mu}\cdot\boldsymbol{R}(\gamma_R)\cdot\boldsymbol{e}_i. \tag{5}$$

Here $\boldsymbol{e}_i$ is $\boldsymbol{e}_x$, $\boldsymbol{e}_y$, or $\boldsymbol{e}_z$ and it denotes the polarization of the ith electric field in the space-fixed coordinate system. The maximal field strength is given by $\mathcal{E}_i$, and $u_i(t) = s_i(t)\cos(\omega_i t + \phi_i)$ is the time dependence of the electric field with the dimensionless envelope $s_i(t)$, frequency ω_i, and phase ϕ_i. The molecular dipole moment $\boldsymbol{\mu} = (\mu_a, \mu_b, \mu_c)^T$ is given in molecule-fixed coordinates, and the rotation matrix $\boldsymbol{R}(\gamma_R)$ transforms between the space-fixed and molecule-fixed coordinate system. It depends on the Euler angles $\gamma_R = (\theta, \psi, \varphi)$. The components of the dipole moment μ_α, $\alpha = a, b, c$, are functions of the nuclear coordinates, i.e., the normal mode χ. The interaction with the electric field thus couples molecular vibrations with the rotational degrees of freedom.

Upon excitation with electric fields, a rovibrational wave packet of the form

$$|\psi(t)\rangle = \sum_j\sum_{\nu} c_{\nu,j}(t)|\nu\rangle|\phi_j\rangle \tag{6}$$

is excited. We now consider an operator that acts only on the vibrational subspace, e.g., the coordinate $\hat{\chi}$ of a normal mode of the molecule. The expectation value of $\hat{\chi}$, which includes integrating over the rotational degrees of freedom, is then given by

$$\langle\hat{\chi}\rangle(t) = \langle\psi(t)|\hat{\chi}|\psi(t)\rangle = \sum_j\sum_{\nu,\nu'} c_{\nu,j}(t)c^*_{\nu',j}(t)\langle\nu'|\hat{\chi}|\nu\rangle. \tag{7}$$

Inserting $\hat{\chi} = \sqrt{\frac{\hbar}{2m\omega}}(\hat{a} + \hat{a}^\dagger)$, where m is the reduced mass and $\omega = (E_1^{\mathrm{vib}} - E_0^{\mathrm{vib}})/\hbar$ the normal-mode frequency, the expectation value can be written as

$$\langle\hat{\chi}\rangle(t) = \sqrt{\frac{\hbar}{2m\omega}}\sum_j \mathrm{Re}\left(\sum_{\nu}\sqrt{\nu+1}c_{\nu,j}(t)c^*_{\nu+1,j}(t)\right), \tag{8}$$

where we assume that the relevant vibrational states can be approximated by a harmonic-oscillator wave function. The expectation value is nonzero only if the rovibrational states with ν and $\nu+1$ belong to the same rotational state j. For an ensemble of molecules, a nonzero expectation value $\langle\hat{\chi}\rangle(t) \neq 0$ means that all molecules vibrate in phase despite their random orientation in space, forming a coherent vibrational wave packet. The coupling to the rotational motion thus imposes additional conditions for the excitation of coherent vibrational motion if the molecules are randomly oriented.

For simplicity, we consider in the following a vibrational wave packet that consists of the ground and first excited vibrational states only, as shown in Fig. 1(a). This implies a slight anharmonicity in the vibrational potential so that the energy gaps between subsequent vibrational states are not the same and it is thus possible to address the transition between $|0\rangle$ and $|1\rangle$ without driving the transition between $|1\rangle$ and $|2\rangle$ and so on. In this case, the expectation value for the elongation becomes

$$\langle\hat{\chi}\rangle(t) = \sqrt{\frac{\hbar}{2m\omega}}\sum_j \mathrm{Re}[b_{0,j}(t)b^*_{1,j}(t)\exp(i\omega t)], \tag{9}$$

where $b_{\nu,j}(t) = c_{\nu,j}(t)\exp[i(E_{\nu}^{\mathrm{vib}} + E_j^{\mathrm{rot}})t/\hbar]$. The elongation along the normal mode becomes maximal with $\langle\hat{\chi}\rangle_{\max} = \frac{1}{2}\sqrt{\frac{\hbar}{2m\omega}}$ if the population is equally distributed between the ground and excited vibrational state for each rotational state j.

In this paper we discuss the excitation of vibrational wave packets in a planar molecule, for example COFCl (see Fig. 1), where the molecular plane is the only symmetry element. The normal mode can describe either an in-plane vibration, which we denote by $\chi = \zeta$ [see Fig. 1(c)], or an out-of-plane vibration $\chi = \xi$ [as shown in Fig. 1(e)]. Excitation of an in-plane vibrational wave packet leaves a planar molecule achiral.

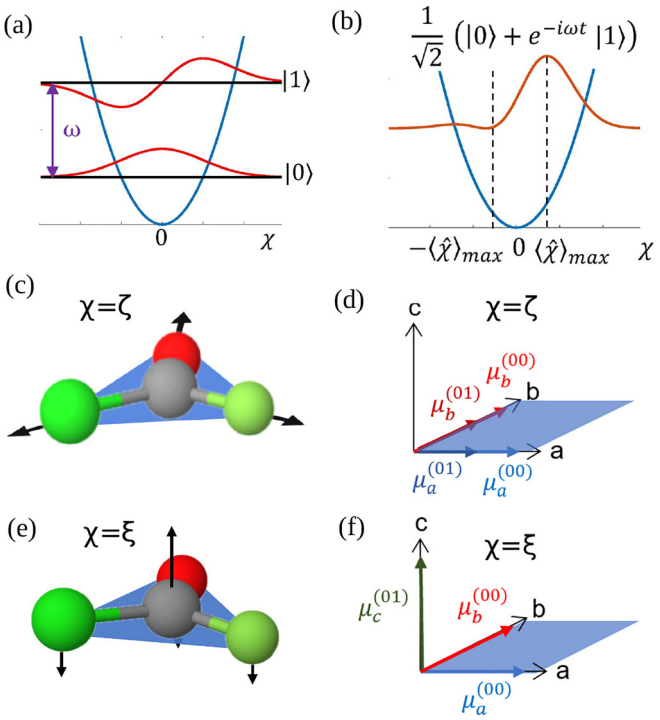

FIG. 1. Creation of a vibrational wave packet in a planar molecule for the example of COFCl. (a) Vibrational eigenstates $|0\rangle$ and $|1\rangle$ of a normal mode χ. (b) Vibrational wave packet as superposition of eigenstates $|0\rangle$ and $|1\rangle$. (c) Sketch of an in-plane normal mode $\chi = \zeta$ of COFCl. (d) Permanent dipole moment of COFCl with components $\mu_a^{(00)}$ and $\mu_b^{(00)}$ lying in the molecular plane. For the in-plane vibration, the transition dipole moment with components $\mu_a^{(01)}$ and $\mu_b^{(01)}$ lies also in the molecular plane. (e) Sketch of the out-of plane normal mode $\chi = \xi$ of COFCl. (f) Permanent dipole moment with components $\mu_a^{(00)}$ and $\mu_b^{(00)}$ lying in the molecular plane. The transition dipole moment for the out-of plane vibration with component $\mu_c^{(01)}$ perpendicular to the molecular plane.

Vibrations along the out-of-plane normal mode ξ break the planar symmetry [26]. If a wave packet with $\langle\hat{\xi}\rangle(t) \neq 0$ is excited, the molecule becomes temporarily chiral and oscillates between its two enantiomeric structures with the frequency of the out-of-plane vibration.

In the following, we discuss different interaction schemes for the excitation of coherent vibrational wave packets in randomly oriented molecules. In Sec. III A we make use of symmetry properties of asymmetric top rotors to derive conditions for the external fields $\mathbf{E}_i(t)$ so that after excitation $\langle\hat{\chi}\rangle(t) \neq 0$, i.e., the average elongation measured for an ensemble of molecules does not vanish. This rather technical part is followed by Sec. III B, where the results of Sec. III A are illustrated with examples for the creation of achiral and chiral wave packets in planar molecules. In Sec. III C we address the question of full controllability of the Schrödinger equation (2) as a means to defining conditions for external fields that can induce maximal molecular response $\langle\hat{\chi}\rangle = \langle\hat{\chi}\rangle_{\max}$ for any given initial condition. In Secs. IV and V we then concentrate on inducing chirality in an achiral molecule and present two examples for the excitation of chiral vibrational wave packets.

TABLE I. Character table of D_2, the molecular rotation group for asymmetric top molecules, and transformation properties of the asymmetric top eigenfunctions [33]. The transformation properties of the rotational states depend on whether the quantum numbers K_a and K_c are even (e) or odd (o).

D_2	E	R_a^π	R_b^π	R_c^π	K_aK_c
A	1	1	1	1	ee
B_a	1	1	−1	−1	eo
B_b	1	−1	1	−1	oo
B_c	1	−1	−1	1	oe

III. CONDITIONS FOR CREATING A COHERENT VIBRATIONAL WAVE PACKET

A. Symmetry of the rovibrational wave functions

According to Eq. (9), for the simplest case of two vibrational states forming a coherent superposition, a net chiral signal after averaging over rotations is obtained if the coefficients $b_{0,j}(t)$ and $b_{1,j}(t)$ are nonzero. Vanishing of these coefficients due to symmetry arguments can be determined by using perturbation theory to solve the time-dependent Schrödinger equation (2). Starting from the initial state $|\psi(0)\rangle = |\nu_0\rangle|\phi_{j_0}\rangle$ and considering resonant transitions, the coefficients $b_{\nu,j}(t)$ are not identically zero only if

$$\begin{aligned}&\langle\phi_j|\langle\nu|H_{\rm int}^l|\nu_0\rangle|\phi_{j_0}\rangle\\ &\quad= \langle\phi_j|\langle\nu|H_{\rm int}|\nu^{(l-1)}\rangle|\phi_{j^{(l-1)}}\rangle\cdots\\ &\qquad\times\langle\phi_{j''}|\langle\nu''|H_{\rm int}|\nu'\rangle|\phi_{j'}\rangle\langle\phi_{j'}|\langle\nu'|H_{\rm int}|\nu_0\rangle|\phi_{j_0}\rangle\neq 0\end{aligned}\quad(10)$$

for at least one $l = 0, 1, 2, \ldots$, where l is the order of perturbation and $|\phi_{j'}\rangle|\nu'\rangle$, $|\phi_{j''}\rangle|\nu''\rangle$, and so on, are arbitrary intermediate rovibrational states. Since a nonzero expectation value $\langle\hat{\chi}\rangle(t)$ in Eq. (9) requires both $b_{0,j}(t)$ and $b_{1,j}(t)$ to be nonzero, the following condition has to be fulfilled: For a given initial rotational state $|\phi_{j_0}\rangle$ and $|\nu_0\rangle = |0\rangle$, at least one j must exist for which both transition matrix elements

$$\langle\phi_j|\langle 0|H_{\rm int}^l|0\rangle|\phi_{j_0}\rangle \neq 0, \quad(11a)$$

$$\langle\phi_j|\langle 1|H_{\rm int}^{l'}|0\rangle|\phi_{j_0}\rangle \neq 0 \quad(11b)$$

are nonzero for at least one l and l'.

Next we analyze what Eq. (11) implies for vibrating asymmetric top rotors. We represent the rotational part of the rovibrational wave function in the basis of asymmetric top eigenfunctions $|\phi_j\rangle = |J_{K_a,K_c}, M\rangle$, with $J = 0, 1, 2, \ldots$ the rotational quantum number, $M = -J, -J+1, \ldots, J$ the projection quantum number for rotation around the space-fixed axis, and $K_a = 0, 1, \ldots, J$ ($K_c = 0, 1, \ldots, J$) the projection quantum number for rotation around the molecular axis of a prolate (oblate) symmetric top.[1] The symmetry of the rovibrational wave functions with respect to the space-fixed and molecule-fixed coordinate systems determines whether the

[1]Each asymmetric top eigenfunction is uniquely described by J, M, and the two corresponding symmetric top quantum numbers K_a and K_c. Since the rotational energy eigenvalues $E_j^{\rm rot} = E_{J_{K_a,K_c}}^{\rm rot}$ do not depend on M, we denote the rotational energy levels by J_{K_a,K_c}.

transitions matrix elements in Eq. (11) are nonzero. Symmetry with respect to the space-fixed frame results in the (usual) M-selection rules for electric dipole interaction: $\Delta M = 0$ for transitions induced by z-polarized fields and $\Delta M = \pm 1$ for transitions induced by x- or y-polarized fields. Since both conditions in Eq. (11) need to be fulfilled, the polarizations $\mathbf{e}_i$ of the external fields $\mathbf{E}_i(t)$ have to be chosen such that for the lth-order process in Eq. (11a) the final quantum number M is the same as for the l'th-order process in Eq. (11b). We will discuss this condition for several examples in Sec. III B.

Equation (11) also involves the symmetry of the rovibrational wave functions with respect to the molecule-fixed frame. The corresponding condition can be obtained from the properties of the symmetry group D_2 of an asymmetric top, recalled in Table I [33]: The transition matrix elements [Eq. (11)] can be nonzero only if they transform according to the totally symmetric irreducible representation of D_2, i.e.,

$$\Gamma(|\phi_j\rangle) \times \Gamma(\langle 0|H_{\rm int}|\nu^{(l-1)}\rangle) \times \cdots \times \Gamma(\langle \nu''|H_{\rm int}|\nu'\rangle) \times \Gamma(\langle \nu'|H_{\rm int}|0\rangle) \times \Gamma(|\phi_{j_0}\rangle) = A, \tag{12a}$$

$$\Gamma(|\phi_j\rangle) \times \Gamma(\langle 1|H_{\rm int}|\lambda^{(l'-1)}\rangle) \times \cdots \times \Gamma(\langle \lambda''|H_{\rm int}|\lambda'\rangle) \times \Gamma(\langle \lambda'|H_{\rm int}|0\rangle) \times \Gamma(|\phi_{j_0}\rangle) = A \tag{12b}$$

for conditions (11a) and (11b), respectively, where $\nu', \ldots, \nu^{(l-1)}, \lambda', \ldots, \lambda^{(l'-1)} \in \{0, 1\}$. According to Table I, the irreducible representations of the rotational wave functions are $\Gamma(|\phi_j\rangle) = \Gamma(|J_{K_a,K_c}, M\rangle) = A$ or B_α, with $\alpha = a, b, c$, depending only on the values of K_a and K_c. In Eq. (12) we have further utilized that $B_\alpha \times B_\alpha = A$.

Finally, Eq. (11) needs to be evaluated for the vibrational part. In order to determine the irreducible representations of the vibrational transition matrix elements in Eq. (11), we decompose the interaction Hamiltonian into its irreducible components. Therefore, we consider an electric field $\mathbf{E} = \mathbf{e}_p \mathcal{E} u(t)$ with polarization $\mathbf{e}_p$, amplitude $\mathcal{E}$, and time dependence $u(t)$.[2] The vibrational transition matrix elements can be written as

$$\begin{aligned}\langle \nu'|H_{\rm int}|\nu\rangle &= \sum_\alpha \langle \nu'|H_{{\rm int},\alpha}|\nu\rangle \\ &= -\mathcal{E}u(t) \sum_\alpha \mu_\alpha^{(\nu'\nu)} R_{\alpha,p}(\gamma_R),\end{aligned} \tag{13}$$

with $\alpha = a, b, c$ and $\mu_\alpha^{(\nu\nu')} = \langle \nu'|\mu_\alpha|\nu\rangle$. Here $\mu_\alpha^{(01)} = \mu_\alpha^{(10)}$ are transition dipole moments. For the permanent dipole moments we assume for simplicity that $\mu_\alpha^{(11)} = \mu_\alpha^{(00)}$. The matrix elements of the rotational matrix $\boldsymbol{R}(\gamma_R)$ are denoted by $R_{\alpha,p}(\gamma_R)$. The irreducible components of the interaction Hamiltonian transform according to the irreducible representations of D_2 (Table I), namely,

$$\langle \nu'|H_{{\rm int},a}|\nu\rangle \sim B_a, \tag{14a}$$

$$\langle \nu'|H_{{\rm int},b}|\nu\rangle \sim B_b, \tag{14b}$$

$$\langle \nu'|H_{{\rm int},c}|\nu\rangle \sim B_c \tag{14c}$$

(see the Appendix). In order to obtain nonvanishing coefficients $b_{0,j}(t)$ and $b_{1,j}(t)$, the excitation process has to contain an lth-order process with

$$\Gamma(\langle 0|H_{\rm int}|\nu^{(l-1)}\rangle) \times \cdots \times \Gamma(\langle \nu'|H_{\rm int}|0\rangle) = \Gamma_0, \tag{15}$$

where Γ_0 is one of the irreducible representations of D_2, and an l'th-order process that fulfills

$$\Gamma(\langle 1|H_{\rm int}|\lambda^{(l'-1)}\rangle) \times \cdots \times \Gamma(\langle \lambda'|H_{\rm int}|0\rangle) = \Gamma_0 \tag{16}$$

with the same Γ_0. Equations (12a) and (12b) are thus both fulfilled if $\Gamma(|\phi_j\rangle) \times \Gamma_0 \times \Gamma(|\phi_0\rangle) = A$, i.e., the final rotational state $|\phi_j\rangle$ transforms according to $\Gamma(|\phi_j\rangle) = \Gamma(|\phi_0\rangle) \times \Gamma_0$. In combination with Eq. (14), the conditions (15) and (16) can be utilized to determine which combination of external fields $\mathbf{E}_i$ is capable of exciting a coherent vibrational wave packet in initially randomly oriented molecules.

B. Examples of creating coherent rovibrational wave packets

We now show how to use the conditions just derived to create coherent vibrational wave packets, both achiral and chiral. To this end, we consider a planar molecule, with the molecular plane as the only symmetry element, e.g., COFCl, as shown in Fig. 1. Due to the planar symmetry, the molecule has a permanent dipole moment in the molecular plane, i.e., $\mu_a^{(00)} \neq 0$ and $\mu_b^{(00)} \neq 0$ while $\mu_c^{(00)} = 0$. For an in-plane vibration $\chi = \zeta$, also the transition dipole moment lies in the molecular plane, i.e., $\mu_a^{(01)} \neq 0$, $\mu_b^{(01)} \neq 0$, and $\mu_c^{(01)} = 0$ [see Fig. 1(d)]. For an out-of-plane vibration $\chi = \xi$, the transition dipole moment is perpendicular to the molecular plane, i.e., $\mu_a^{(01)} = 0$, $\mu_b^{(01)} = 0$, and $\mu_c^{(01)} \neq 0$, as in Fig. 1(f) (see also Ref. [26]). In the following, we discuss various excitation scenarios, assuming that the molecules are initially in their vibrational and rotational ground state $|0\rangle|\phi_0\rangle = |0\rangle|0_{0,0}, 0\rangle$.

Scenario (a). Rovibrational excitation in first-order perturbation theory, i.e., excitation of a vibrational state with one IR photon, is described by the case $l = 0$ and $l' = 1$. This reduces the condition (11a) to $\langle \phi_j|\phi_{j_0}\rangle \neq 0$, which requires $j = j_0$. For $l' = 1$ and $j = j_0$, the condition (11b) can only be fulfilled if $\Gamma(\langle 1|H_{\rm int}|0\rangle) = A$. However, this is in contradiction to Eq. (14). It is thus not possible to excite a vibrational wave packet with $\langle \hat{\chi}\rangle \neq 0$ with a single IR interaction in a sample of randomly oriented molecules. The same result is obtained when the molecular rotation is treated classically [26]. In both cases, it corresponds at any instant of time to as many molecules (each with a given orientation) with $+\langle \hat{\chi}\rangle$ as with $-\langle \hat{\chi}\rangle$ such that the overall normal-mode elongation vanishes when averaged over random orientations.

[2]For a set of electric fields $\mathbf{E}_i$ [Eq. (3)], an additional sum over i is required.

Scenario (b). Next we consider the case $l = 1$ and $l' = 1$. The conditions (15) and (16) are then fulfilled if $\mu_\alpha^{(01)} \neq 0$ and $\mu_\alpha^{(00)} \neq 0$ for the same α, i.e., if both the transition dipole moment and the permanent dipole moment have a nonvanishing component along the same molecular axis. This is the case if the normal mode is an in-plane vibration $\chi = \zeta$ with $\mu_a^{(00)}$ and $\mu_a^{(01)}$ or with $\mu_b^{(00)}$ and $\mu_b^{(01)}$ [see Fig. 1(d)]. A purely rotational transition within the vibrational ground state with $\langle 0|H_{\rm int}|0\rangle \neq 0$ can be realized with a microwave field resonant to an allowed rotational transition. The vibrational transition with $\langle 1|H_{\rm int}|0\rangle \neq 0$ can be driven by an IR pulse resonant to the frequency of the normal mode. In addition, the overall excitation must fulfill the M-selection rules. Starting from the rotational state $|\phi_0\rangle = |0_{0,0}, 0\rangle$, the transitions described by Eq. (11), namely, $\langle J_{K_a,K_c}, M|\langle 0|H_{\rm int}|0\rangle|0_{0,0}, 0\rangle$ and $\langle J_{K_a,K_c}, M|\langle 1|H_{\rm int}|0\rangle|0_{0,0}, 0\rangle$, must both end in the same rotational state M. Since one can always choose the quantization axis, we can assume, without loss of generality, the first interaction to be with a z-polarized field, inducing rotational transitions with $\Delta M = 0$. Then $M = 0$, and the second field also has to be z polarized such that the condition (11b) is fulfilled with $M = 0$. Thus, an achiral vibrational wave packet with $\langle\hat{\xi}\rangle \neq 0$ can be excited with a combination of a z-polarized microwave pulse and an IR pulse with the same polarization. However, excitation of a chiral vibrational wave packet is not possible.

Scenario (c). In order to induce a chiral vibrational wave packet, it is necessary to excite the out-of plane vibrational mode $\chi = \xi$. In this case, the transition dipole moment is perpendicular to the permanent dipole moment [see Fig. 1(f)]. The lowest order for which the conditions (15) and (16) can be fulfilled in this case is for $l = 2$ and $l' = 1$ (or vice versa) with

$$\Gamma(\langle 0|H_{{\rm int},a}|0\rangle) \times \Gamma(\langle 0|H_{{\rm int},b}|0\rangle) = B_a \times B_b = B_c \tag{17}$$

and

$$\Gamma(\langle 1|H_{{\rm int},c}|0\rangle) = B_c. \tag{18}$$

In other words, three interactions are required, transforming according to the irreducible representations B_a, B_b, and B_c, respectively. Equation (17) describes purely rotational transitions within the vibrational ground state which can be realized with two microwave pulses, while the vibrational transition (18) can be driven by an IR pulse. We discuss such an excitation scheme in Sec. IV. Exchanging the roles of l and l', the condition (15) can also be fulfilled by

$$\Gamma(\langle 0|H_{{\rm int},a}|1\rangle) \times \Gamma(\langle 1|H_{{\rm int},b}|0\rangle) = B_a \times B_b = B_c. \tag{19}$$

Equation (19) together with Eq. (18) describes the conditions for exciting a chiral wave packet with three rovibrational transitions, which can be driven by three IR pulses. For a planar molecule in free space, $\langle 0|H_{{\rm int},\alpha}|1\rangle = 0$ for $\alpha = a, b$. In Sec. V we show that such transition matrix elements do occur in the presence of an external static electric field.

Moreover, the above conditions imply that the three electric fields that are (at least) necessary to excite a chiral vibrational wave packet have to be polarized orthogonally to each other. Starting with $M_0 = 0$ and assuming without loss of generality that the first-order transition $\langle\phi_j|\langle 1|H_{{\rm int},c}|0\rangle|\phi_0\rangle$ is driven by a z-polarized field, the final rotational state has the quantum numbers $J = J_0 + 1 = 1$ and $M = M_0 = 0$. This rotational state can be addressed by a second-order process only with a combination of x- and y-polarized fields [14]. Note that this corresponds exactly to the general condition for distinguishing enantiomers when exciting molecules that are chiral in the first place [32]. It has also been determined as condition for creating a chiral wave packet when considering a classical angular distribution of the rotors [26].

C. Controllability of the rovibrational Schrödinger equation

The conditions discussed in Secs. III A and III B ensure that a coherent vibrational wave packet can be created starting from the ground rovibrational state. In order to ensure that a coherent vibrational wave packet with maximal elongation $\langle\hat{\chi}\rangle_{\rm max}$ can be excited from an arbitrary initial state, we pursue a different approach, namely, we analyze the controllability [34]. The Schrödinger equation is said to be controllable if the system can be steered from any given initial condition to any given target state, with a suitable choice of control fields $\mathbf{E}_i(t)$, $i = 1, \ldots, f$. This implies that one can create a target state corresponding to maximal elongation $\langle\hat{\chi}\rangle$.

In order to analyze the controllability of the rovibrational Schrödinger equation (2) we make use of graph theory based methods [36,43,46]. We consider a graph $\mathcal{G}$ consisting of the eigenstates $|\nu\rangle|\phi_j\rangle$ of H_0 as nodes and the nonzero transition matrix elements $\langle\phi_j|\langle\nu|H_{\rm int}|\nu'\rangle|\phi_{j'}\rangle$ as edges. A quantum system has been shown to be controllable if the associated graph $\mathcal{G}$ has a connected subgraph that contains all nodes of $\mathcal{G}$ and only decoupled transitions [44].[3] Here two transitions are called coupled by a control Hamiltonian if they are nonvanishing and have equal energy gaps. A transition is uncoupled if for any other transition there exists at least one control Hamiltonian that does not couple them. Finally, a transition is decoupled if for any other transition there exists at least one nested commutator (of arbitrary length) between control and drift Hamiltonians that does not couple them [46]. For a quantum rotor, most transitions are coupled due to the degeneracy of the rotational states. Recently, a graph-theoretic method to decouple the resonant transitions between asymmetric top states was developed [41] and the maximal number of external fields required to control finite subsystems of an asymmetric top was identified [40]. Here we generalize these methods to analyze the controllability of the rovibrational Schrödinger equation (2). However, controllability analysis requires an *a priori* selection of controls, i.e., external fields that interact with the molecule, in contrast to symmetry analysis. We carry out controllability analysis for two practical examples in Secs. IV and V, focusing on the excitation of a chiral vibrational wave packet under the conditions derived in scenario (c) in Sec. III B. In particular, in Sec. IV we study the interaction of a planar molecule with a combination of microwave pulses and an IR pulse, whereas

[3] Actually, this condition implies a stronger notion of controllability, namely, controllability at the level of the propagators, which implies, in particular, controllability of the density matrices.

in Sec. V we consider the interaction with a sequence of IR pulses in the presence of a static electric field. We exemplify in both cases that the symmetry conditions derived in scenario (c) in Sec. III B are fulfilled and then prove controllability to ascertain that the excitation process can result in a maximal chiral response, irrespective of the initial state.

IV. EXCITATION WITH A COMBINATION OF MICROWAVE AND IR PULSES

In the first example, microwave pulses are employed to induce transitions between rotational states of an asymmetric top molecule and IR radiation is applied to produce an excited vibrational state of the out-of-plane normal mode.

The Hamiltonian describing the interaction with microwave and IR pulses in the electric dipole approximation reads

$$H_{\rm int}(t) = H_{\rm int}^{\rm mw}(t) + H_{\rm int}^{\rm IR}(t). \tag{20}$$

The interaction of the microwave pulses with the electric fields $\mathbf{E}_i(t)$ as defined in Eq. (3) is then given by

$$H_{\rm int}^{\rm mw}(t) = \sum_i u_i(t) H_i^{\rm mw}, \tag{21}$$

with

$$H_i^{\rm mw} = -\mathcal{E}_i \sum_{j,j'} \sum_{\nu=0}^{1} |\nu\rangle|\phi_{j'}\rangle\langle\phi_{j'}| \times [\boldsymbol{\mu}^{(00)} \cdot \mathbf{R}(\gamma_R) \cdot \boldsymbol{e}_i]|\phi_j\rangle\langle\phi_j|\langle\nu| + \text{c.c.} \tag{22}$$

The transformation between the space-fixed and molecule-fixed coordinate system can be expressed in terms of the Wigner D-matrix elements $D^J_{MK}(\gamma_R)$ [47] as

$$\begin{aligned}
\boldsymbol{\mu}^{(00)} \cdot \mathbf{R}(\gamma_R) \cdot \boldsymbol{e}_x &= \frac{\mu_a^{(00)}}{\sqrt{2}}\left(D^1_{-10} - D^1_{10}\right) \\
&\quad + \frac{\mu_b^{(00)}}{2}\left(D^1_{11} - D^1_{1-1} - D^1_{-11} + D^1_{-1-1}\right), \\
\boldsymbol{\mu}^{(00)} \cdot \mathbf{R}(\gamma_R) \cdot \boldsymbol{e}_y &= -\mathrm{i}\frac{\mu_a^{(00)}}{\sqrt{2}}\left(D^1_{-10} + D^1_{10}\right) \\
&\quad + \mathrm{i}\frac{\mu_b^{(00)}}{2}\left(D^1_{11} - D^1_{1-1} + D^1_{-11} - D^1_{-1-1}\right), \\
\boldsymbol{\mu}^{(00)} \cdot \mathbf{R}(\gamma_R) \cdot \boldsymbol{e}_z &= \mu_a^{(00)} D^1_{00} - \frac{\mu_b^{(00)}}{\sqrt{2}}\left(D^1_{01} - D^1_{0-1}\right).
\end{aligned} \tag{23}$$

The evaluation of the matrix elements $\langle\phi_{j'}|\boldsymbol{\mu}^{(00)}\mathbf{R}(\gamma_R)\boldsymbol{e}_p|\phi_j\rangle$ between the asymmetric top eigenstates $|\phi_j\rangle = |J_{K_a,K_c}, M\rangle$ is described, e.g., in [14,40]. The time dependence of the microwave pulses can be written as $u_i(t) = s_i(t)\cos(\omega_i t + \phi_i)$, where $s_i(t)$ is the dimensionless envelope and ω_i and ϕ_i are the frequency and phase of the field. The frequencies ω_i are chosen to be resonant to one of the rotational transitions. The field intensity can then be tuned such that only those transitions resonant to the frequency of the field are excited [40] and $\langle\phi_{j'}|\boldsymbol{\mu}^{(00)} \cdot \mathbf{R}(\gamma_R) \cdot \boldsymbol{e}_i|\phi_j\rangle = 0$ if $\omega_i \neq |E_j^{\rm rot} - E_{j'}^{\rm rot}|/\hbar$.

The frequency of the IR pulse is chosen such that it is (approximately) resonant to the transition between the vibrational states $|0\rangle$ and $|1\rangle$, that is, only transitions between the vibrational states can occur, but no rotational transitions within one of the vibrational states. The corresponding interaction Hamiltonian can thus be expressed as

$$H_{\rm int}^{\rm IR}(t) = u(t)\hat{H}^{\rm IR}, \tag{24}$$

with

$$\hat{H}^{\rm IR} = -\mathcal{E}_{\rm IR} \sum_{j,j'} |0\rangle|\phi_{j'}\rangle\langle\phi_{j'}| \times [\boldsymbol{\mu}^{(01)} \cdot \mathbf{R}(\gamma_R) \cdot \boldsymbol{e}_{\rm IR}]|\phi_j\rangle\langle\phi_j|\langle 1| + \text{c.c.}, \tag{25}$$

where $\boldsymbol{e}_{\rm IR}$ denotes the polarization of the IR pulse. Recall that the transition dipole moment has only one component perpendicular to the molecular plane, i.e., only $\mu_c^{(01)} \neq 0$. The transformation from the space-fixed to the molecule-fixed frame is thus given by [47]

$$\begin{aligned}
\boldsymbol{\mu}^{(01)}\mathbf{R}(\gamma_R)\boldsymbol{e}_x &= -\mathrm{i}\frac{\mu_c^{(01)}}{2}\left(D^1_{11} + D^1_{1-1} - D^1_{-11} - D^1_{-1-1}\right), \\
\boldsymbol{\mu}^{(01)}\mathbf{R}(\gamma_R)\boldsymbol{e}_y &= \frac{\mu_c^{(01)}}{2}\left(D^1_{11} + D^1_{1-1} + D^1_{-11} + D^1_{-1-1}\right), \\
\boldsymbol{\mu}^{(01)}\mathbf{R}(\gamma_R)\boldsymbol{e}_z &= \mathrm{i}\frac{\mu_c^{(01)}}{\sqrt{2}}\left(D^1_{01} + D^1_{0-1}\right).
\end{aligned} \tag{26}$$

The time dependence of the IR pulse can be written as $u(t) = s(t)\cos(\omega_{\rm IR}t + \phi)$. If the duration of the IR pulse is longer that the rotational period of the molecule, its bandwidth is small enough to selectively excite individual rovibrational states, i.e., only transitions with $\omega_{\rm IR} = |E_{j'}^{\rm rot} + E_0^{\rm vib} - E_j^{\rm rot} - E_1^{\rm vib}|/\hbar$. However, the bandwidth of a short IR pulse can be large enough to excite several rotational states simultaneously. In this case the interaction Hamiltonian contains all transition matrix elements which are allowed according to the dipole selection rules.

In the following, we show that the combination of microwave and IR pulses fulfills the requirements derived in scenario (c) in Sec. III B for the creation of a chiral wave packet. We analyze the controllability of the rovibrational Schrödinger equation (2) with an interaction Hamiltonian of the form (20) and discuss the results of numerical simulations demonstrating the excitation of a chiral wave packet with a combination of microwave and IR pulses.

A. Conditions for exciting a chiral wave packet

The conditions for creating a chiral vibrational wave packet with a combination of microwave and IR pulses can be deduced directly from scenario (c) in Sec. III B. With the two components of the permanent dipole moment, $\mu_a^{(00)}$ and $\mu_b^{(00)}$, the condition (17) is fulfilled with two microwave pulses, one resonant to a b-type transition, e.g., from level $J_{K_a,K_b} = 0_{0,0}$ to $1_{1,1}$, and the second one resonant to an a-type transition, e.g., $1_{1,1} \to 1_{1,0}$ within the vibrational ground state $|0\rangle$. The condition (18) is fulfilled since the transition dipole moment has the nonvanishing component $\mu_c^{(01)}$ which drives the transition from $|0\rangle \to |1\rangle$ and $0_{0,0} \to 1_{1,0}$. Moreover, as shown in scenario (c) in Sec. III B, three orthogonal polarization directions are required, e.g., a z-polarized IR pulse and x- and y-polarized microwave pulses.

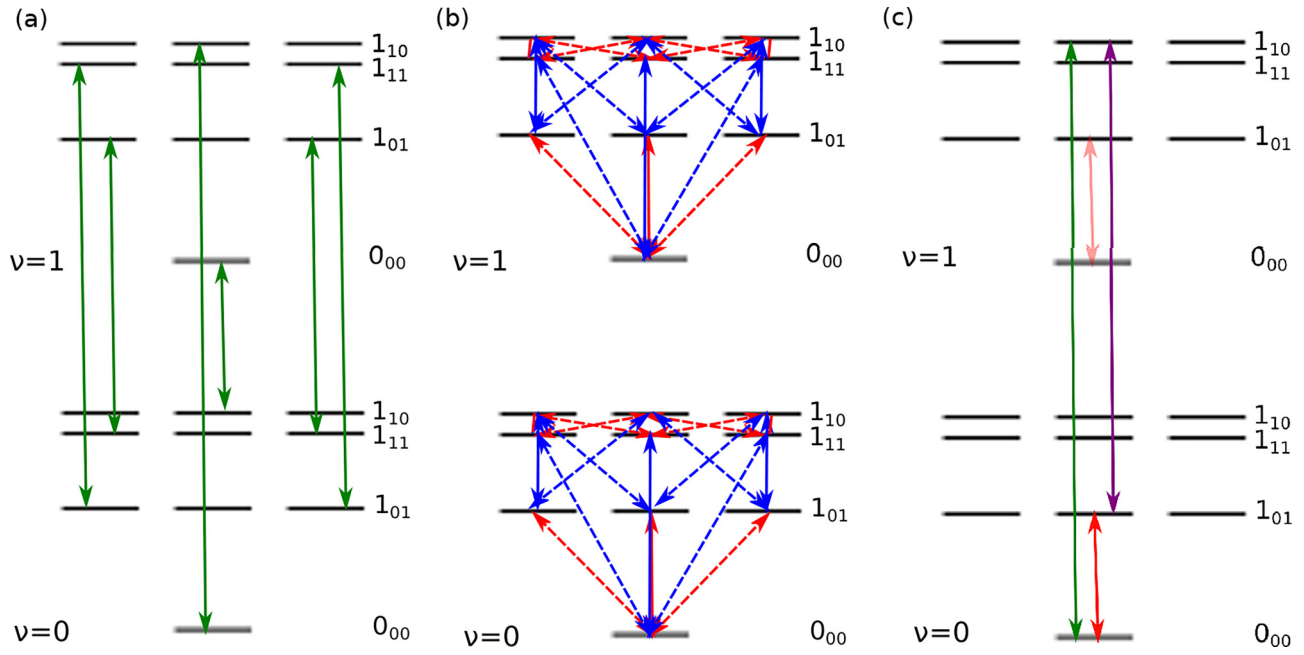

FIG. 2. Graph with asymmetric top eigenstates as nodes (horizontal lines) and transition matrix elements as edges (green, red, and blue arrows). (a) Interaction with a z-polarized IR pulse (green arrows). (b) Interaction with x-, y-, and z-polarized microwave pulses. Red arrows indicate transition matrix elements $\langle\phi_j'|\mu_a^{(00)}|\phi_j\rangle$ and blue arrows correspond to transition matrix elements $\langle\phi_j'|\mu_b^{(00)}|\phi_j\rangle$. (c) Graphical commutator between the transitions indicated by the green and red arrows, allowing the two coupled transitions indicated by the red arrows to decouple.

B. Controllability analysis

We now demonstrate that the Schrödinger equation (2) with an interaction Hamiltonian of the form (20) is controllable, implying that maximal elongation can be obtained for an arbitrary initial state. We first consider a subspace of the asymmetric top eigenstates consisting of all rotational states with quantum numbers $J = 0$ and 1. The corresponding graph is shown in Fig. 2, where the nodes of the graph, i.e., the rovibrational eigenstates $|\nu\rangle|\phi_j\rangle$, are indicated by horizontal black lines. The green lines in Fig. 2(a) show the transition matrix elements (edges) induced by the control Hamiltonian $\hat{H}^{IR}$. It can be seen that the graph is not connected, i.e., it is not possible to reach, from an arbitrary initial state, all other states of the system by following the edges. Thus, the system is not controllable with a single IR pulse. The edges corresponding to the microwave pulses [Eq. (22)] are shown in Fig. 2(b), where all three polarization directions x, y, and z are considered. The red and blue lines correspond to transitions driven by $\mu_a^{(00)}$ and $\mu_b^{(00)}$, respectively. A finite-dimensional subsystem including the eigenstates of at least two consecutive values of J of a single quantum asymmetric top is controllable with x-, y-, and z-polarized fields via electric dipole interaction if the rotor exhibits two orthogonal components of the permanent dipole moment [42]. Since COFCl has two orthogonal dipole moment components in the molecular plane, the rotational part of the Hamiltonian, i.e., the lower graph in Fig. 2(b), is controllable. This means that each of the edges (red and blue lines) corresponds to a decoupled transition. The graph of the rovibrational system consists of two identical rotational subsystems, shifted by the vibrational energy. By interaction with microwave fields alone, this system is not controllable since the graph is not connected [see Fig. 2(b)]. Moreover, each transition in the lower rotational subsystem is coupled to the corresponding transition in the upper rotational subsystem. Note that this is strictly true only if rovibrational coupling is neglected, as we assume here.

In order to show that the rovibrational system is controllable with a combination of a (z-polarized) IR pulse and x-, y-, and z-polarized microwave pulses, we have to show that the combined graph containing all transitions shown in Figs. 2(a) and 2(b) is connected and contains only uncoupled or decoupled transitions. It is easy to see that the graph is connected if one of the edges in Fig. 2(a) is added to the graph shown in Fig. 2(b), e.g., the transition between the states $|0\rangle|0_{00}, 0\rangle$ and $|1\rangle|1_{10}, 0\rangle$ [green line in Fig. 2(c)]. The corresponding transition is uncoupled because there exists no other transition with the same energy gap. What remains is to show that the pairs of coupled transitions [identical transitions in the upper and lower parts of Fig. 2(b)] can be decoupled. This can be proven by using graphical commutators [41,46]. Note that the commutator between an $N \times N$ matrix with a single pair of nonzero elements (n, m) and (m, n) with an $N \times N$ matrix with nonzero elements (n, k) and (k, n) with $n \neq m \neq k$ is a matrix with nonzero elements (m, k) and (k, m). If the nonzero matrix elements present edges of a graph, the edge (m, k) between the nodes m and k is called the graphical commutator of (n, m) and (n, k) [46]. Figure 2(c) shows the graphical commutator between the (decoupled) transition $|0\rangle|0_{00}, 0\rangle \leftrightarrow |1\rangle|1_{10}, 0\rangle$ (green line) and the pair of coupled transitions $|\nu\rangle|0_{00}, 0\rangle \leftrightarrow |\nu\rangle|1_{01}, 0\rangle$, $\nu = 0, 1$ (red lines). The resulting commutator is indicated by the purple line. The graphical commutator between the green and

purple edges then results in the lower red line, corresponding to the transition $|0\rangle|0_{00},0\rangle \leftrightarrow |0\rangle|1_{01},0\rangle$. By this procedure, we have shown that the transition $|0\rangle|0_{00},0\rangle \leftrightarrow |0\rangle|1_{01},0\rangle$ is decoupled from $|1\rangle|0_{00},0\rangle \leftrightarrow |1\rangle|1_{01},0\rangle$. Having decoupled one pair of coupled transitions, all other pairs can also become decoupled by again taking (graphical) commutators between a decoupled transition and a pair of coupled transitions. This allows us to conclude that the Schrödinger equation for the rovibrational interaction with a combination of an IR pulse with three microwave fields is controllable. Note that in Fig. 2 we only show the rotational states with $J = 0$ and 1. However, since every finite-dimensional rotational subsystem including the eigenstates of at least two consecutive values of J of an asymmetric top is controllable [42], the result is also valid for larger rotational subsystems. We have thus shown that the time-dependent Schrödinger equation with the interaction Hamiltonian (20) is controllable for the out-of-plane vibration of COFCl with a combination of a z-polarized IR pulse and three orthogonally polarized microwave pulses, implying that maximal elongation $\langle\hat{\xi}\rangle_{\max}$ can be obtained with such a set of pulses for an arbitrary initial state.

According to Secs. III B and IV A, two microwave pulses, polarized in the x and y directions in combination with a z-polarized IR pulse, are already sufficient to obtain a chiral signal, although not necessarily the maximal possible, if the initial state is the rovibrational ground state. In Sec. IV C we make use of this simpler condition to numerically demonstrate the excitation of a chiral wave packet with a combination of microwave and IR pulses.

C. Chiral rovibrational dynamics

To demonstrate the excitation of a chiral wave packet with a combination of microwave and IR pulses numerically, we consider the simplest initial condition describing randomly oriented rotors, i.e., we assume that the molecules are initially in their ground vibrational and rotational state $|\psi(0)\rangle = |0\rangle|0_{00},0\rangle$. As an example, we consider COFCl molecules [26] with rotational constants $A = 11781.84$ MHz, $B = 5246.37$ MHz, and $C = 3627.49$ MHz and dipole moments $\mu_a^{(00)} = -1.1$ D and $\mu_b^{(00)} = 0.8$ D.

As shown in Sec. IV A, the excitation of a chiral wave packet requires two microwave pulses polarized in the x and y directions, respectively. The population dynamics in the vibrational ground state during the interaction with microwave pulses, obtained by numerically solving the time-dependent Schrödinger equation (2) with interaction Hamiltonian (20), is shown in Fig. 3. The duration of the first microwave pulse is chosen such that 50% of the population remains in the ground state $|0\rangle|0_{00},0\rangle$ while 25% is transferred to each of the states $|0\rangle|1_{11},\pm1\rangle$. The second pulse then completely transfers the population of the states $|0\rangle|1_{11},\pm1\rangle$ to $|0\rangle|1_{10},0\rangle$ so that the wave function after excitation with the microwave pulses reads

$$|\psi(t)\rangle = \frac{1}{\sqrt{2}}(|0_{00},0\rangle + \exp[i\phi(t)]|1_{10},0\rangle)|0\rangle, \tag{27}$$

with the dynamical phase $\phi(t) = -(E_{1_{10}} - E_{0_{00}})t/\hbar + \tilde{\phi}$, where $E_{J_{K_a,K_c}}$ are the energies of the asymmetric top eigenstates and $\tilde{\phi} = \phi_2 - \phi_1$ is the relative phase between the microwave fields. The vibrational state $|1\rangle$ is excited by a z-polarized IR pulse. Figure 4 displays the excitation with a narrowband IR pulse with

$$u(t) = \exp\left(-\frac{(t-t_0)^2}{2\Delta t^2}\right)\cos(\omega_L t + \phi), \tag{28}$$

$\omega_L = \omega + E_{1_{10}}/\hbar$, and a bandwidth $\Delta\omega = 1/\Delta t$ small enough to excite only the transition from $|0_{00},0\rangle|0\rangle$ to $|1_{10},0\rangle|1\rangle$. The resulting population dynamics is shown in Figs. 4(a) and 4(b). Figure 4(c) shows the envelope of the elongation $\langle\hat{\xi}\rangle(t)$ which emerges during the interaction with the IR pulse and oscillates with the vibrational frequency ω. For COFCl, $\omega \approx 607$ B [26] and the vibrational period is thus $T \approx 0.01t_0$. The elongation becomes maximal if the population is equally distributed between pairs of rovibrational states $|0\rangle|\phi_j\rangle$ and $|1\rangle|\phi_j\rangle$ [see Eq. (9)]. Therefore, the pulse length and field strength are chosen such that after the excitation $|b_{0j}|^2 = |b_{1j}|^2 = \frac{1}{2}$ for $j = 1_{10}, 0$ [red dotted lines in Fig. 4(a)] and all other coefficients are zero. This results in a chiral vibrational wave packet with maximal elongation $\langle\hat{\xi}\rangle_{\max}/\xi_0 = \frac{1}{2}$ with $\xi_0 = \sqrt{\hbar/2m\omega}$ as shown in Fig. 4(c). The phase of the oscillation depends on the relative phase between the electric fields. The excitation process thus requires a stable constant phase between the microwave and IR pulses.

To induce a chiral wave packet, it is however not necessary to selectively excite a single rovibrational state. As shown in Fig. 5, a chiral wave packet can also be excited by a short broadband IR pulse. As before, we assume that the rotational wave function (27) has been created by microwave excitation. According to the rovibrational selection rules, the IR pulse drives transitions between $|0\rangle|0_{00},0\rangle$ and $|1\rangle|1_{10},0\rangle$ as well as between $|0\rangle|1_{10},0\rangle$ and $|1\rangle|0_{00},0\rangle$ [see Figs. 5(a) and 5(b)]. Choosing the pulse duration and intensity of the IR pulse such that there is population in all four states after the end of pulse leads to nonvanishing terms in Eq. (9). The corresponding expectation value $\langle\xi\rangle/\xi_0$ is shown in Fig. 5(c). The

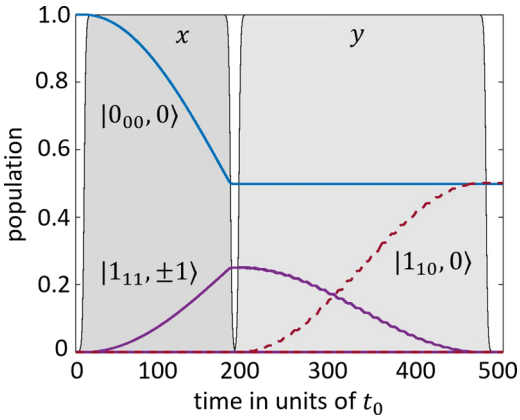

FIG. 3. Excitation of a rotational wave packet in $v = 0$ with two microwave pulses. The population dynamics is shown for the rotational states $|0_{00},0\rangle$ (blue solid line), $|1_{11},\pm1\rangle$ (magenta solid line), and $|1_{10},0\rangle$ (red dashed line). The envelope of the two microwave pulses is indicated by the gray shapes; they are x and y polarized as indicated in the figure. Time is given in units of $t_0 = \hbar/B \approx 30$ ps. The amplitude of the microwave fields is $\mathcal{E}_i = 2 \times 10^4$ V/m for the three fields $i = 1, 2, 3$.

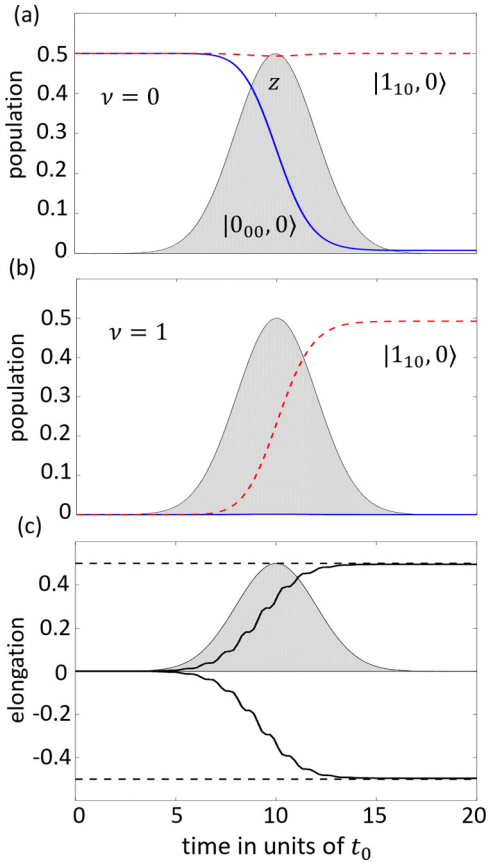

FIG. 4. Population dynamics after excitation with a long z-polarized IR pulse. Population is shown in the (a) ground and (b) excited vibrational states. The blue solid and red dashed lines correspond to the rotational states $|0_{00}, 0\rangle$ and $|1_{10}, 0\rangle$, respectively. (c) Envelope of elongation $\langle\hat{\xi}\rangle(t)/\xi_0$ during the excitation with the IR pulse. [The oscillation of $\langle\hat{\xi}\rangle(t)$ with $T = 0.01t_0$ is too fast compared to the timescale of the plot to be resolved.] The maximal elongation $\pm\langle\hat{\xi}\rangle_{\max}/\xi_0$ is indicated by the horizontal dashed lines. In all panels, the envelope of the IR pulse is indicated by the gray shapes; the maximal amplitude is $\mathcal{E}_{\mathrm{IR}} = 5 \times 10^5$ V/m.

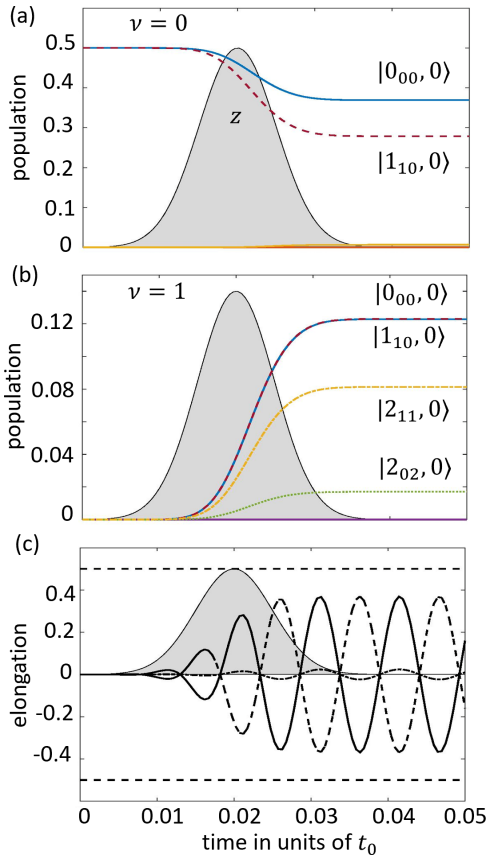

FIG. 5. Population dynamics after excitation with a short z-polarized IR pulse for the (a) ground and (b) excited vibrational states. The blue solid and red dashed lines correspond to the rotational states $|0_{00}, 0\rangle$ and $|1_{10}, 0\rangle$, respectively, and the yellow dash-dotted and green dotted lines correspond to $|2_{11}, 0\rangle$ and $|2_{02}, 0\rangle$, respectively. (c) Elongation $\langle\hat{\xi}\rangle(t)/\xi_0$ due to the excitation with the IR pulse. The solid, dashed, and dash-dotted lines correspond to $\phi = \pi/2$, $-\pi/2$, and 0, respectively. The envelope of the IR pulse is indicated by the gray shapes; the maximal amplitude is $\mathcal{E}_{\mathrm{IR}} = 7.5 \times 10^7$ V/m.

average elongation of the out-of-plane coordinate depends on the dynamical phase ϕ. For $\phi = 0$, the average elongation is close to zero, since the contributions to $\langle\xi\rangle$ from the rotational states $|0_{00}, 0\rangle$ and $|1_{10}, 0\rangle$ cancel each other. For $\phi = \pm\pi/2$, the contributions from the rotational states $|0_{00}, 0\rangle$ and $|1_{10}, 0\rangle$ add constructively, and $\langle\xi\rangle$ changes its phase if one switches from $\phi = \pi/2$ to $\phi = -\pi/2$. Thus the relative phases between the microwave and IR pulses must be constant during the interaction.

It should be noted that the IR pulse also drives transitions between the initial state $|0\rangle|1_{10}, 0\rangle$ and the rovibrational states $|1\rangle|2_{11}, 0\rangle$ and $|1\rangle|2_{02}, 0\rangle$ [see yellow and green lines in Fig. 4(b)]. Since the corresponding states $|0\rangle|2_{11}, 0\rangle$ and $|0\rangle|2_{02}, 0\rangle$ are not populated, these states do not contribute to the average elongation of the out-of-plane coordinate and, as a result, the maximal elongation of the chiral wave packet is smaller than $\frac{1}{2}$.

We have numerically demonstrated the excitation of a chiral vibrational wave packet with two microwave pulses, polarized in the x and y directions and one z-polarized IR pulse for a molecule that is initially in its ground rotational and vibrational state. In an experiment, the initial condition will typically contain a (thermal) distribution of rotational states. In this case, the pulse sequences shown here will induce some chiral signal, but it might be small depending on the initial rotational temperature. However, the controllability analysis in Sec. IV B shows that it is always possible to induce a chiral wave packet with maximal elongation. In this case, three microwave fields polarized in the x, y, and z directions might be necessary to induce maximal elongation as well as more complicated pulse shapes of the microwave and IR pulses.

Another experimental challenge for the creation of a chiral wave packet with microwave and IR pulses is that the phase between the microwave fields and the IR fields must be stable, which can be realized, e.g., by using a frequency comb. To avoid phase locking between microwave and infrared pulses, a chiral wave packet can also be excited without involving microwave pulses. In Sec. V we demonstrate how to create a chiral vibrational wave packet with a static electric field and a sequence of IR pulses.

V. EXCITATION WITH IR PULSES IN THE PRESENCE OF A STATIC ELECTRIC FIELD

In this example, we consider planar molecules evolving under the influence of the time-dependent Schrödinger equation

$$i\hbar\frac{\partial}{\partial t}|\psi(t)\rangle = [H_0 + \epsilon H_{\rm stat} + H_{\rm int}(t)]|\psi(t)\rangle, \tag{29}$$

where

$$H_{\rm stat} = -\mathcal{E}_0\boldsymbol{\mu}^{(00)}\cdot\mathbf{R}(\gamma_R)\cdot\boldsymbol{e}_z \tag{30}$$

describes the interaction with a static electric field in the z direction. Here the field strength is defined as $\mathcal{E} = \epsilon\mathcal{E}_0$, where $\mathcal{E}_0$ is a unit field strength and ϵ a small dimensionless number indicating that the interaction with the static field is small compared to the molecular Hamiltonian H_0. The transformation between the space-fixed and molecule-fixed coordinate systems is given by Eq. (23). The interaction with the IR pulses can be written as

$$H_{\rm int}(t) = \sum_i u_i(t)H_i^{\rm IR}, \tag{31}$$

with

$$H_i^{\rm IR} = -\mathcal{E}_i\sum_{j,j'}|0\rangle|\phi_{j'}\rangle\langle\phi_{j'}|\boldsymbol{\mu}^{(01)}\cdot\mathbf{R}(\gamma_R)\cdot \times \boldsymbol{e}_i|\phi_j\rangle\langle\phi_j|\langle 1| + \text{c.c.}, \tag{32}$$

where $\mathbf{E} = \mathbf{e}_i\mathcal{E}_i u_i(t)$ is the electric field of the IR pulse with polarization $\mathbf{e}_i$, amplitude $\mathcal{E}_i$, and time dependence $u_i(t) = s_i(t)\cos(\omega_i t + \phi_i)$. In Sec. V A we show that the Schrödinger equation (29) fulfills the conditions necessary to induce a chiral vibrational wave packet, as discussed in Sec. III B. In Sec. V B we analyze the controllability of the Schrödinger equation (29) and in Sec. V C we numerically demonstrate the excitation of a chiral wave packet with a sequence of three IR pulses in the presence of a static electric field.

A. Conditions for creating a chiral wave packet

As demonstrated in scenario (c) in Sec. III B, a vibrational wave packet can be excited by three IR pulses with x, y, and z polarization under the condition that the excitation path contains transition matrix elements with $\langle 1|H_{{\rm int},\alpha}|0\rangle \neq 0$ for $\alpha = a$, b, and c, respectively. Since the transition dipole moment for the out-of-plane vibration of a planar molecule is perpendicular to the molecular plane, only the component $\mu_c^{(01)}$ is nonzero. Thus, IR pulses only induce transition matrix elements of the form $\langle 1|H_{{\rm int},c}|0\rangle$ and excitation of a chiral wave packet with only IR pulses is not possible without additional external fields. However, in the presence of a static field, additional rovibrational transitions occur, which are forbidden under field-free conditions. In order to determine the nonvanishing transition matrix elements in the presence of a static electric field, we consider the interaction with the static field as a perturbation and describe the field-dressed rotational states $|\phi_j^{\rm FD}\rangle$, i.e., the eigenstates of $H_0 + \epsilon H_{\rm stat}$. Using the selection rules associated with $H_{\rm stat}$, one obtains by first-order perturbation theory that

$$|\phi_j^{\rm FD}\rangle = |\phi_j\rangle + \epsilon|\phi_j'\rangle + O(\epsilon), \tag{33}$$

with

$$|\phi_j'\rangle = \sum_{k\neq j}\frac{\langle\phi_j|H_{\rm stat}|\phi_k\rangle}{E_j^{\rm rot} - E_k^{\rm rot}}|\phi_k\rangle, \tag{34}$$

where only those values of k are considered for which $E_j^{\rm rot} \neq E_k^{\rm rot}$. Note that Eqs. (33) and (34) hold even if the eigenvalue corresponding to $|\phi_j\rangle$ is degenerate: Indeed, the total Hilbert space splits into the direct sum of $H_{\rm stat}$-invariant subspaces (each of them identified by the quantum number M), to which the eigenstates $|\phi_j\rangle$ belong, and in each of these subspaces H_0 has a simple spectrum. The transition matrix elements between the field-dressed rotational states in first-order perturbation theory then read

$$\begin{aligned}\langle\phi_k^{\rm FD}|\langle 1|H_i^{\rm IR}|0\rangle|\phi_j^{\rm FD}\rangle &= \langle\phi_k|\langle 1|H_i^{\rm IR}|0\rangle|\phi_j\rangle \\ &+ \epsilon\big(\langle\phi_k'|\langle 1|H_i^{\rm IR}|0\rangle|\phi_j\rangle + \langle\phi_k|\langle 1|H_i^{\rm IR}|0\rangle|\phi_j'\rangle\big) \\ &+ O(\epsilon).\end{aligned} \tag{35}$$

Since the permanent dipole moment of COFCl has components $\mu_a^{(00)} \neq 0$ and $\mu_b^{(00)} \neq 0$, the interaction with the static field can be decomposed into $H_{\rm stat} = H_{{\rm stat},a} + H_{{\rm stat},b}$, and $H_i^{\rm IR} = H_{i,c}^{\rm IR}$. Inserting Eq. (34), we obtain

$$\begin{aligned}\langle\phi_k|\langle 1|H_i^{\rm IR}|0\rangle|\phi_j'\rangle = &\sum_{l\neq j}\frac{1}{E_j^{\rm rot} - E_l^{\rm rot}}\langle\phi_k|\langle 1|H_{i,c}^{\rm IR}|0\rangle|\phi_l\rangle \\ &\times\langle\phi_l|\langle 0|H_{{\rm stat},a}|0\rangle|\phi_j\rangle \\ &+\sum_{l\neq j}\frac{1}{E_j^{\rm rot} - E_l^{\rm rot}}\langle\phi_k|\langle 1|H_{i,c}^{\rm IR}|0\rangle|\phi_l\rangle \\ &\times\langle\phi_l|\langle 0|H_{{\rm stat},b}|0\rangle|\phi_j\rangle.\end{aligned} \tag{36}$$

The direct products of the irreducible representations of D_2 are $B_c \times B_a = B_b$ and $B_c \times B_b = B_a$ (see Table I). Therefore, transitions between the field-dressed states driven by IR pulses are governed in first-order perturbation by matrix elements that transform according to B_a and B_b while transition matrix elements between the unperturbed rotational states transform according to B_c. Thus, the conditions for creating a vibrational wave packet with nonvanishing elongation $\langle\hat{\xi}\rangle$ are fulfilled if the molecules interact with three IR pulses polarized orthogonally to each other in the presence of a static electric field.

B. Controllability analysis

In order to ensure that a maximal chiral signal can be obtained from an arbitrary initial condition, we also study the controllability of the Schrödinger equation (29) using first-order perturbation theory in combination with graphical methods. We therefore introduce a graph $\mathcal{G}$ whose nodes are the eigenstates $|\phi_j\rangle|\nu\rangle$ (see horizontal lines in Fig. 6). The edges of the graph are defined by the transition matrix elements between the field-dressed eigenstates [Eq. (35)], i.e., by the zeroth-order couplings $\langle\phi_k|\langle 1|H_i^{\rm IR}|0\rangle|\phi_j\rangle$ and the first-order couplings $\langle\phi_k'|\langle 1|H_i^{\rm IR}|0\rangle|\phi_j\rangle + \langle\phi_k|\langle 1|H_i^{\rm IR}|0\rangle|\phi_j'\rangle$. To analyze the controllability, it is convenient to choose the polarizations $i = \sigma_+, \sigma_-$, where $\sigma_+ = x + iy$ and $\sigma_- = x - iy$ instead of $i = x, y$. The Schrödinger equation (29) is con-

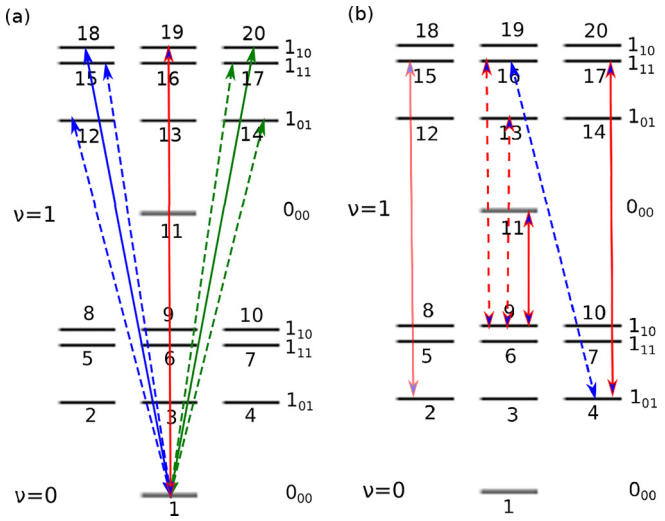

FIG. 6. Graph with rovibrational states $|J_{k_a,K_c}, M\rangle|\nu\rangle$, $\nu = 0, 1$, as nodes and zeroth-order (solid lines) and first-order (dashed lines) transition matrix elements as edges. The red, green, and blue arrows correspond to transitions induced by control fields with $i = z$, σ_+, and σ_-, respectively. For convenience, the nodes are numbered from 1 to 20. (a) All nonvanishing transitions connecting node 1. (b) An additional set of nonvanishing transitions that is necessary to connect node 1 to all nodes greater than or equal to 11.

trollable if the graph $\mathcal{G}$ has a subgraph containing all nodes and only uncoupled or decoupled transitions. It should be noted that if the system is controllable with control fields with $i = z, \sigma_+, \sigma_-$ it is controllable as well with a set of fields with linear polarizations $i = x, y, z$.

A way to prove controllability is to draw all edges, i.e., all nonzero zeroth- and first-order transition matrix elements, and analyze if the graph $\mathcal{G}$ is connected by uncoupled or decoupled transitions. It is however more convenient to start with a smaller subgraph and subsequently add as many edges as are necessary to prove that the graph is connected. Therefore, we first analyze all transitions with the ground state $|0\rangle|\phi_0\rangle = |0\rangle|0_{0,0}, 0\rangle$, as indicated in Fig. 6. To simplify the notation, we number the nodes of the graph, starting from 1 for the ground state $|0\rangle|0_{0,0}, 0\rangle$ to 20 for the state $|1\rangle|1_{0,1}, 1\rangle$ (see Fig. 6). A z-polarized IR pulse induces the zeroth-order transition $1 \leftrightarrow 19$, indicated by the red solid line in Fig. 6(a). Fields with $i = \sigma_+$ induce transitions with $\Delta M = +1$, i.e., the zeroth-order transition $1 \leftrightarrow 20$ and the first-order transitions $1 \leftrightarrow 14$ and $1 \leftrightarrow 17$, which are determined by Eq. (36). Likewise, fields with $i = \sigma_-$ induce transitions with $\Delta M = -1$, i.e., the transitions $1 \leftrightarrow 18$, $1 \leftrightarrow 15$, and $1 \leftrightarrow 12$. All those transitions are decoupled since those transitions corresponding to the same control Hamiltonian (same polarization) have different energy gaps.

Next we show that node 1 is also connected with nodes 11, 13, and 16. Note that there are no zeroth- or first-order transitions matrix elements that directly connect vortex 1 with any of these states. We add the edges $9 \leftrightarrow 11$, $9 \leftrightarrow 13$, $9 \leftrightarrow 16$, $2 \leftrightarrow 15$, $4 \leftrightarrow 17$, and $4 \leftrightarrow 16$, which are shown in Fig. 6(b), to the subgraph. All edges represented by red arrows are induced by a z-polarized control field, with $9 \leftrightarrow 11$, $2 \leftrightarrow 15$, and $4 \leftrightarrow 17$ being zeroth-order transitions while $9 \leftrightarrow 13$ and $9 \leftrightarrow 16$ are first-order transitions, as it can be verified with help of Eq. (36). The zeroth-order transition $4 \leftrightarrow 16$ is induced by a control field with polarization $i = \sigma_-$. Since the subgraph contains the edge $1 \leftrightarrow 17$ [see Fig. 6(a)], the additional edges couple vortex 1 with 16, 13, and 11. Note that the transitions $2 \leftrightarrow 15$ and $4 \leftrightarrow 17$ are induced by the same control field ($i = z$) and have the same energy gap. They are thus coupled. By taking the graphical commutator between the transitions $1 \leftrightarrow 17$ and $4 \leftrightarrow 17$, one can however decouple the transitions $2 \leftrightarrow 15$ and $4 \leftrightarrow 17$ [46]. The subgraph consisting of all edges shown in Figs. 6(a) and 6(b) thus contains only decoupled transitions. Node 1 is thus connected to all nodes in the upper part of the graph, i.e., for all states in the excited vibrational states $|\nu = 1\rangle$. Finally, we show that node 11 is connected with all nodes smaller than or equal to 10; it suffices to do it symmetrically, that is, replace 1 with 11 and any state $n \geqslant 11$ with $n - 10$. The subgraph we have described satisfies the desired properties: It is a connected graph consisting of only uncoupled or decoupled transitions. This proves that the corresponding Schrödinger equation (29) is controllable. Controllability of Eq. (29) implies that with a combination of a static field and a set of x, y, and z or σ_+, σ_-, and z polarized IR pulses, a chiral wave packet with maximal elongation can be created.

The interaction between the molecule and a static field is typically much smaller than the rotational energies, that is, we consider the regime $\epsilon \ll 1$. We therefore treat the resulting transition matrix elements in first-order perturbation theory. However, since eigenvalues and eigenvectors of $H_0 + \epsilon H_{\text{stat}}$ are analytic functions of the parameter ϵ and analytic functions have at worst isolated zeros (when they are not identically zero), the controllability result holds for almost every value of the parameter ϵ.

C. Chiral rovibrational dynamics in a static field

In order to simulate the rovibrational dynamics in the presence of a static electric field, we first numerically determine the field-dressed eigenstates $|\phi_j^{\text{FD}}\rangle|\nu\rangle$, i.e., the eigenstates of $H_0 + \epsilon H_{\text{stat}}$ for $\epsilon = 0.3$, which corresponds to a field strength of $\mathcal{E} = 10^6$ V/m. Similar to Sec. IV C, we assume that the molecule is initially in the field-dressed rovibrational ground state $|\psi(0)\rangle = |0\rangle|\phi_0^{\text{FD}}\rangle$ and simulate the population dynamics during the interaction with three orthogonally polarized IR pulses by numerically integrating the Schrödinger equation (29). Figures 7(a) and 7(b) display the population in the ground and excited vibrational states, respectively. The corresponding excitation mechanism is sketched in Fig. 8. The first pulse is x polarized and has a Gaussian shape with central frequency $\omega_1 = \omega + (E^{\text{rot}}_{1_{10}} - E^{\text{rot}}_{0_{00}})/\hbar$. The allowed transitions are indicated by the solid and dashed arrows in Fig. 8(a). The green solid arrow represents the transitions matrix elements between the field-free rotational states and the dashed arrows show the much weaker transitions resulting from couplings between rotational states in the presence of the static field. The strength and width of the pulse are chosen such that only the transition resonant to ω_1 is driven and 50% of the population remains in the ground rovibrational state (blue line in Fig. 7) and 25% is transferred to the states $|1\rangle|1_{10}, \pm 1\rangle$ each. Note that this is a pure c-type transition. To fulfill the

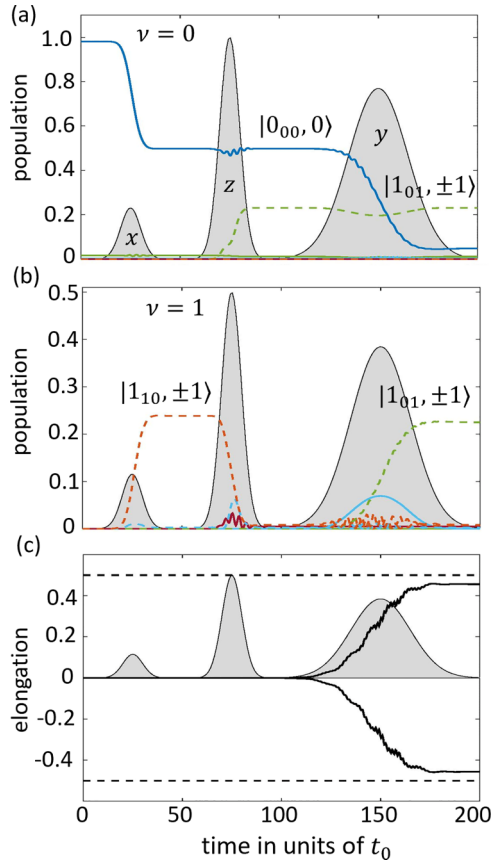

FIG. 7. Population dynamics for excitation with a sequence of three IR pulses in the presence of a static electric field. Population is shown in the (a) ground and (b) excited vibrational states. The blue, red, and green lines correspond to the rotational states $|0_{00}, 0\rangle$, $|1_{10}, \pm 1\rangle$, and $|1_{01}, \pm 1\rangle$, respectively. (c) Envelope of the elongation $\langle\xi\rangle(t)/\xi_0$. The dashed lines indicate the maximal elongation $\langle\xi\rangle/\xi_0 = \pm 1/2$. In all panels, the envelopes of the pulses are indicated by the gray shapes; the maximal amplitude is $\mathcal{E}_i = 1.5 \times 10^5$, 6.5×10^5, and 5×10^5 V/m for $i = 1$, 2, and 3, respectively. The polarization of the pulses is denoted by x, y, and z. Note that the population dynamics is shown in the field-free basis.

conditions for the creation of a chiral wave packet, the other two pulses have to drive a- and b-type transitions, which arise only due to the couplings induced by the static field and are thus much weaker. The integrated field intensity of these pulses is therefore much larger (see gray shapes in Fig. 7). The second pulse is z polarized, has a central frequency $\omega_2 = \omega + (E^{\rm rot}_{1_{10}} - E^{\rm rot}_{1_{01}})/\hbar$, and drives the transitions from $|1\rangle|1_{10}, \pm 1\rangle$ to $|0\rangle|1_{01}, \pm 1\rangle$, which is a b-type transition [see red dashed arrow in Fig. 8(b)]. Finally, the third, y-polarized pulse transfers the remaining ground state population to $|1\rangle|1_{01}, \pm 1\rangle$ by an a-type transition [blue dashed arrows in Fig. 8(c)] and thus creates the chiral wave packet.

The envelope of the elongation $\langle\hat{\xi}\rangle(t)/\xi_0$ is shown in Fig. 7(c). The elongation oscillates with frequency ω (with $T = 2\pi/\omega \approx 0.01 t_0$ the oscillation is too fast to be resolved on the timescale shown in Fig. 7). Since this pulse sequence transfers almost the complete population to the two pairs of states $|0\rangle|1_{01}, \pm 1\rangle$ and $|1\rangle|1_{01}, \pm 1\rangle$, the elongation reaches almost its maximal value $\langle\hat{\xi}\rangle/\xi_0 = \pm\frac{1}{2}$. Note that in the third step, the transition between $|0\rangle|0_{00}, 0\rangle$ and $|1\rangle|1_{01}, \pm 1\rangle$ can also be induced by a second x-polarized pulse. However, in that case the vibrational wave packet created by the pair of states $|0\rangle|1_{01}, +1\rangle$ and $|1\rangle|1_{01}, +1\rangle$ oscillates out of phase with the wave packet consisting of the states $|0\rangle|1_{01}, -1\rangle$ and $|1\rangle|1_{01}, -1\rangle$ and thus the net elongation becomes zero.

We have thus demonstrated numerically that a chiral wave packet can be excited with a combination of three IR pulses polarized orthogonally to each other if a static electric field induces transitions between rovibrational states which are forbidden under field-free conditions. In this case, the relative phases between the three IR pulses have to be constant, which is easier to realize experimentally than phase locking between microwave and IR pulses.

VI. CONCLUSION

With the help of symmetry considerations and controllability analysis, we have derived requirements for electromagnetic fields interacting in an electric dipole approximation with randomly oriented molecules that allow for the excitation of coherent vibrational motion. For the controllability analysis, we extended graph-theoretic methods derived for quantum asymmetric tops [40,41] to rovibrational systems. Perturbation theory for controllability in the presence of a static field is usually considered to lift spectral degeneracies; see, e.g., [39] for such an analysis in rotating symmetric top molecules. Here we pursued a different approach, where perturbation theory for controllability in the presence of a static field is considered to create additional couplings in the matrix elements, which graphically represent additional edges of the quantum spectral graph.

We applied this methodology to determine conditions for the creation of chiral vibrational wave packets in achiral molecules. In order to measure the chirality of the excited molecule, i.e., to measure the time-dependent elongation along the out-of-plane mode, all excitation processes described here could be combined with vibrationally resolved photoelectron circular dichroism, as proposed in [26]. The conditions for creating chiral vibrational wave packets had been derived earlier by taking a classical rotational average of an ensemble of randomly oriented molecules, where the rotation is assumed to be frozen during the excitation process [26]. The quantum-mechanical derivation shown here extends this treatment to cases where molecules rotate during the excitation process. This allows us to compare conditions for creating (temporal) chirality in regimes where molecular rotations behave classically and quantum mechanically. The excitation schemes proposed here rely on coherent excitation of individual rotational or rovibrational states, i.e., they require interaction times long enough to resolve the rotational spectrum of molecules. Such transitions can only be described by a quantum-mechanical treatment of molecular rotation.

While the excitation scheme proposed in [26] requires Raman excitation to an excited electronic state, exciting individual rotational states for the creation of a chiral vibrational wave packet occurs only in the electronic ground state of the COFCl molecules. This has the advantage that the dipole and transition dipole moments within the electronic ground states are larger than electronic transition dipole moments.

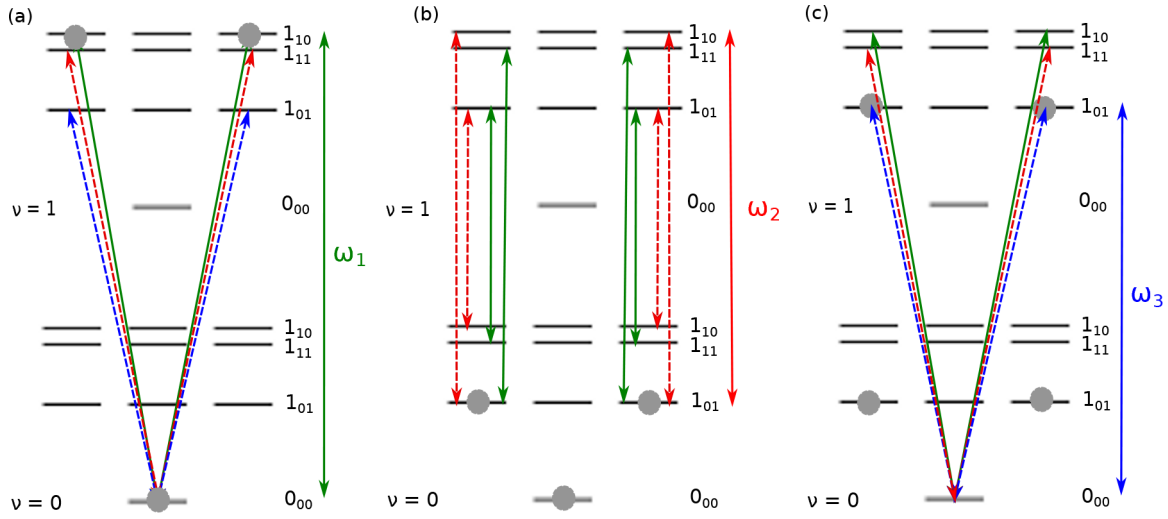

FIG. 8. Transition matrix elements and populated states for the excitation process shown in Fig. 7. The transition matrix elements are shown for the excitation with the IR pulses (a) 1, (b) 2, and (c) 3 of Fig. 7. The solid arrows indicate transition matrix elements between field-free rotational states and dashed arrows correspond to transitions allowed only in the presence of a static electric field. The colors (green, blue, and red) indicate the type of transitions (*a*, *b*, and *c* type). The gray circles show which states are populated at the end of the (a) first, (b) second, and (c) third pulses.

As a proof of principle, we simulated the excitation of chiral wave packets assuming that the molecules are initially in their ground rotational and vibrational state. A more realistic description of experimental conditions is an initial thermal distribution of rotational states, whereas for typical temperatures in molecular beams or buffer gas cooled samples the molecules are predominantly in their vibrational ground state. With the help of controllability analysis, we demonstrated that also for such an initial condition a chiral signal with maximal amplitude can be achieved with the proposed excitation mechanisms. However, in this case the microwave and IR pulses are expected to have more complicated shapes and can be obtained, for example, making use of optimal control theory.

When considering higher temperatures, where rotational states with larger J are involved in the excitation process, rovibrational coupling, neglected in the present study, becomes more relevant. On the one hand, this might lead to dephasing of the rovibrational wave packets and thus to a decrease of the pump-probe signal. On the other hand, rovibrational coupling lifts the symmetry restrictions of the transition matrix elements. This might give rise to additional excitation schemes which are forbidden by symmetry in the regime where rovibrational coupling is negligible. In this case, optimization of the pulse shapes is likely to be even more important in order to ensure the proper synchronization between different quantum pathways.

ACKNOWLEDGMENTS

This study was initiated in inspiring discussions with D. Tikhonov and M. Schnell; we would like to thank M. Schnell for her comments on the manuscript. We gratefully acknowledge financial support from the Deutsche Forschungsgemeinschaft through CRC 1319 ELCH and through the joint ANR-DFG CoRoMo Projects No. 505622963/KO 2301/15-1 and No. ANR-22-CE92-0077-01. M.S. and U.B. also acknowledge the ANR Project Quaco No. ANR-17-CE40-0007-01. E.P. acknowledges the project CONSTAT, supported by the Conseil Régional de Bourgogne Franche-Comté and the European Union through the PO FEDER Bourgogne 2014/2020 programs, the EIPHI Graduate School (Grant No. ANR-17-EURE-0002), the STARS Consolidator grant 2021 "NewSRG" of the University of Padova, and the PNRR MUR Project No. PE0000023-NQSTI.

APPENDIX: TRANSFORMATION PROPERTIES OF THE ROTATION MATRIX

In this Appendix we verify Eq. (14), i.e., we show that the elements of the rotation matrix $R_{\alpha,p}(\gamma_R)$ with molecule-fixed coordinates $\alpha = a, b, c$, space-fixed coordinates $p = x, y, z$, and Euler angles $\gamma_R = \theta, \psi, \varphi$ transform according to the irreducible representations of the rotation group D_2. The elements of the rotation group can be written in terms of Wigner D-matrix elements, namely [47–49],

$$R_{a,x} = -\frac{1}{\sqrt{2}}\left(D^1_{10} - D^1_{-10}\right),$$
$$R_{a,y} = -\frac{i}{\sqrt{2}}\left(D^1_{10} + D^1_{-10}\right), \quad R_{a,z} = D^1_{00}, \tag{A1}$$

as well as

$$R_{b,x} = \frac{1}{2}\left[\left(D^1_{11} - D^1_{1-1}\right) - \left(D^1_{-11} - D^1_{-1-1}\right)\right],$$
$$R_{b,y} = \frac{i}{2}\left[\left(D^1_{11} - D^1_{1-1}\right) + \left(D^1_{-11} - D^1_{-1-1}\right)\right],$$
$$R_{b,z} = -\frac{1}{\sqrt{2}}\left(D^1_{01} - D^1_{0-1}\right) \tag{A2}$$

TABLE II. Effect of the rotations R^π_α, $\alpha = a, b, c$, on the Euler angles according to [33].

R^π_α	θ	φ	ψ
R^π_a	θ	φ	$\psi + \pi$
R^π_b	$\pi - \theta$	$\varphi + \pi$	$2\pi - \psi$
R^π_c	$\pi - \theta$	$\varphi + \pi$	$\pi - \psi$

and

$$R_{c,x} = -\frac{i}{2}\left[\left(D^1_{11} + D^1_{1-1}\right) - \left(D^1_{-11} + D^1_{-1-1}\right)\right],$$
$$R_{c,y} = \frac{1}{2}\left[\left(D^1_{11} + D^1_{1-1}\right) + \left(D^1_{-11} + D^1_{-1-1}\right)\right],$$
$$R_{c,z} = \frac{i}{\sqrt{2}}\left(D^1_{01} + D^1_{0-1}\right), \tag{A3}$$

with

$$D^J_{MK} = \exp(-iM\varphi) d^J_{MK}(\theta) \exp(-iK\psi). \tag{A4}$$

The elements of Wigner's (small) d matrix for $J = 1$ are given by $d^1_{00} = \cos\theta$, $d^1_{10} = -\frac{1}{\sqrt{2}}\sin\theta$, and $d^1_{1\pm1} = \frac{1}{2}(1 \pm \cos\theta)$ and obey the relation

$$d^J_{M'M} = (-1)^{M-M'} d^J_{MM'} = d^J_{-M-M'}. \tag{A5}$$

The rotation group of an asymmetric top $D_2 = \{E, R^\pi_a, R^\pi_b, R^\pi_c\}$ contains, besides the identity E, the elements R^π_α which describe the rotation about the molecular axes $\alpha = a, b, c$ by an angle of π [33]. The effect of these rotations on the Euler angles is shown in Table II. Using Table II, one can show that

$$E D^1_{00} = +D^1_{00},$$
$$R^\pi_a D^1_{00} = +D^1_{00},$$
$$R^\pi_b D^1_{00} = -D^1_{00},$$
$$R^\pi_c D^1_{00} = -D^1_{00}. \tag{A6}$$

Comparing with the character table (Table I), one can conclude that D^1_{00} transforms according to the irreducible presentation B_a. Likewise, one can show that also $D^1_{\pm10}$ transform according to B_a. Together with Eq. (A1), we can thus conclude that the elements of the rotational matrix $R_{a,p}$ transform according to B_a for $p = x, y, z$. Moreover,

$$E D^1_{0\pm1} = +D^1_{0\pm1},$$
$$R^\pi_a D^1_{0\pm1} = -D^1_{0\pm1},$$
$$R^\pi_b D^1_{0\pm1} = -D^1_{0\mp1},$$
$$R^\pi_c D^1_{0\pm1} = +D^1_{0\mp1}, \tag{A7}$$

i.e., neither D^1_{01} nor D^1_{0-1} transforms according to an irreducible representation of D_2, but the linear combination $D^1_{01} - D^1_{0-1}$ transforms according to B_b and $D^1_{01} + D^1_{0-1}$ transforms according to B_c. Similarly, one can show that $D^1_{\pm11} - D^1_{\pm1-1}$ transforms according to B_b and $D^1_{\pm11} + D^1_{\pm1-1}$ transforms according to B_c. Comparing with Eqs. (A2) and (A3), we can conclude that the rotation matrix elements $R_{b,p}$ transform according to B_b and $R_{c,p}$ transform according to B_c for all $p = x, y, z$. In summary, we have demonstrated that $R_{a,p} \sim B_a$, $R_{b,p} \sim B_b$, and $R_{c,p} \sim B_c$, verifying Eq. (14).

[1] C. Lux, M. Wollenhaupt, T. Bolze, Q. Liang, J. Köhler, C. Sarpe, and T. Baumert, Angew. Chem. Int. Ed. **51**, 5001 (2012).

[2] D. Patterson, M. Schnell, and J. M. Doyle, Nature (London) **497**, 475 (2013).

[3] R. Cireasa, A. E. Boguslavskiy, B. Pons, M. C. H. Wong, D. Descamps, S. Petit, H. Ruf, N. Thiré, A. Ferré, J. Suarez, J. Higuet, B. E. Schmidt, A. F. Alharbi, F. Légaré, V. Blanchet, B. Fabre, S. Patchkovskii, O. Smirnova, Y. Mairesse, and V. R. Bhardwaj, Nat. Phys. **11**, 654 (2015).

[4] V. A. Shubert, D. Schmitz, D. Patterson, J. M. Doyle, and M. Schnell, Angew. Chem. Int. Ed. **53**, 1152 (2014).

[5] S. Lobsiger, C. Pérez, L. Evangelisti, K. K. Lehmann, and B. H. Pate, J. Phys. Chem. Lett. **6**, 196 (2015).

[6] A. A. Milner, J. A. M. Fordyce, I. MacPhail-Bartley, W. Wasserman, V. Milner, I. Tutunnikov, and I. S. Averbukh, Phys. Rev. Lett. **122**, 223201 (2019).

[7] J. H. Lee, J. Bischoff, A. O. Hernandez-Castillo, B. Sartakov, G. Meijer, and S. Eibenberger-Arias, Phys. Rev. Lett. **128**, 173001 (2022).

[8] H. Singh, F. E. L. Berggötz, W. Sun, and M. Schnell, Angew. Chem. Int. Ed. **62**, e202219045 (2023).

[9] D. Faccialà, M. Devetta, S. Beauvarlet, N. Besley, F. Calegari, C. Callegari, D. Catone, E. Cinquanta, A. G. Ciriolo, L. Colaizzi, M. Coreno, G. Crippa, G. De Ninno, M. Di Fraia, M. Galli, G. A. Garcia, Y. Mairesse, M. Negro, O. Plekan, P. Prasannan Geetha *et al.*, Phys. Rev. X **13**, 011044 (2023).

[10] R. E. Goetz, T. A. Isaev, B. Nikoobakht, R. Berger, and C. P. Koch, J. Chem. Phys. **146**, 024306 (2017).

[11] P. V. Demekhin, A. N. Artemyev, A. Kastner, and T. Baumert, Phys. Rev. Lett. **121**, 253201 (2018).

[12] I. Tutunnikov, E. Gershnabel, S. Gold, and I. S. Averbukh, J. Phys. Chem. Lett. **9**, 1105 (2018).

[13] K. K. Lehmann, J. Chem. Phys. **149**, 094201 (2018).

[14] M. Leibscher, T. F. Giesen, and C. P. Koch, J. Chem. Phys. **151**, 014302 (2019).

[15] A. F. Ordonez and O. Smirnova, Phys. Rev. A **99**, 043417 (2019).

[16] R. E. Goetz, C. P. Koch, and L. Greenman, Phys. Rev. Lett. **122**, 013204 (2019).

[17] O. Neufeld, D. Ayuso, P. Decleva, M. Y. Ivanov, O. Smirnova, and O. Cohen, Phys. Rev. X **9**, 031002 (2019).

[18] J. Vogwell, L. Rego, O. Smirnova, and D. Ayuso, Sci. Adv. **9**, eadj1429 (2023).

[19] A. Kastner, T. Ring, B. C. Krueger, G. B. Park, T. Schaefer, A. Senftleben, and T. Baumert, J. Chem. Phys. **147**, 013926 (2017).

[20] S. Beaulieu, A. Comby, D. Descamps, B. Fabre, G. A. Garcia, R. Geneaux, A. G. Harvey, F. Legare, Z. Masin, L. Nahon, A. F.

Ordonez, S. Petit, B. Pons, Y. Mairesse, O. Smirnova, and V. Blanchet, Nat. Phys. **14**, 484 (2018).
[21] S. T. Ranecky, G. B. Park, P. C. Samartzis, I. C. Giannakidis, D. Schwarzer, A. Senftleben, T. Baumert, and T. Schaefer, Phys. Chem. Chem. Phys. **24**, 2758 (2022).
[22] A. Comby, D. Descamps, S. Petit, E. Valzer, M. Wloch, L. Pouysegu, S. Quideau, J. Bockova, C. Meinert, V. Blanchet, B. Fabre, and Y. Mairesse, Phys. Chem. Chem. Phys. **25**, 16246 (2023).
[23] D. Baykusheva and H. J. Wörner, Phys. Rev. X **8**, 031060 (2018).
[24] S. R. Domingos, C. Perez, M. D. Marshall, H. O. Leung, and M. Schnell, Chem. Sci. **11**, 10863 (2020).
[25] A. Owens, A. Yachmenev, S. N. Yurchenko, and J. Küpper, Phys. Rev. Lett. **121**, 193201 (2018).
[26] D. S. Tikhonov, A. Blech, M. Leibscher, L. Greeman, M. Schnell, and C. P. Koch, Sci. Adv. **8**, eade0311 (2022).
[27] M. Ilchen, N. Douguet, T. Mazza, A. J. Rafipoor, C. Callegari, P. Finetti, O. Plekan, K. C. Prince, A. Demidovich, C. Grazioli, L. Avaldi, P. Bolognesi, M. Coreno, M. Di Fraia, M. Devetta, Y. Ovcharenko, S. Düsterer, K. Ueda, K. Bartschat, A. N. Grum-Grzhimailo *et al.*, Phys. Rev. Lett. **118**, 013002 (2017).
[28] A. F. Ordonez and O. Smirnova, Phys. Rev. A **99**, 043416 (2019).
[29] A. N. Grum-Grzhimailo, N. Douguet, M. Meyer, and K. Bartschat, Phys. Rev. A **100**, 033404 (2019).
[30] S. Y. Buhmann, S. M. Giesen, M. Diekmann, R. Berger, S. Aull, P. Zahariev, M. Debatin, and K. Singer, New J. Phys. **23**, 083040 (2021).
[31] N. Mayer, S. Patchkovskii, F. Morales, M. Ivanov, and O. Smirnova, Phys. Rev. Lett. **129**, 243201 (2022).
[32] A. F. Ordonez and O. Smirnova, Phys. Rev. A **98**, 063428 (2018).
[33] P. R. Bunker and P. Jensen, *Molecular Symmetry and Spectroscopy* (NRC Research, Ottawa, 1998).
[34] D. D'Alessandro, *Quantum Control and Dynamics* (Chapman and Hall, Boca Raton, 2008).
[35] R. Judson, K. Lehmann, H. Rabitz, and W. Warren, J. Mol. Struct. **223**, 425 (1990).
[36] U. Boscain, M. Caponigro, and M. Sigalotti, J. Differ. Equations **256**, 3524 (2014).
[37] T. Chambrion and E. Pozzoli, Automatica **153**, 111028 (2023).
[38] U. Boscain, E. Pozzoli, and M. Sigalotti, SIAM J. Control Optim. **59**, 156 (2021).
[39] T. Chambrion and E. Pozzoli, IEEE Control Syst. Lett. **6**, 2425 (2022).
[40] M. Leibscher, E. Pozzoli, C. Perez, M. Schnell, M. Sigalotti, U. Boscain, and C. P. Koch, Commun. Phys. **5**, 110 (2022).
[41] E. Pozzoli, M. Leibscher, M. Sigalotti, U. Boscain, and C. P. Koch, J. Phys. A: Math. Theor. **55**, 215301 (2022).
[42] E. Pozzoli, Appl. Math. Optim. **85**, 8 (2022).
[43] U. Boscain, M. Caponigro, T. Chambrion, and M. Sigalotti, Commun. Math. Phys. **311**, 423 (2012).
[44] T. Chambrion, P. Mason, M. Sigalotti, and U. Boscain, Ann. Inst. H. Poincaré Anal. Non Linéaire **26**, 329 (2009).
[45] X. Wang, B. Li, J.-S. Li, I. R. Petersen, and G. Shi, IEEE Trans. Autom. Control **68**, 2277 (2023).
[46] F. Gago-Encinas, M. Leibscher, and C. P. Koch, Quantum Sci. Technol. **8**, 045002 (2023).
[47] R. N. Zare, *Angular Momentum* (Wiley, New York, 1988).
[48] E. P. Wigner, *Group Theory and its Application to the Quantum Mechanics of Atomic Spectra* (Academic, New York, 1962).
[49] M. A. Morrison and G. A. Parker, Aust. J. Phys. **40**, 465 (1987).